Experimental Investigation on Dynamic Responses of Concrete-Filled Steel Tubular Members subjected to Transverse Impact Loads

Effendi, Mahmud Kori
Department of Architecture, Graduate School of Human-Environment Studies, Kyushu University : Doctoral program

Kawaguchi, Hiromitsu
Department of Architecture, Graduate School of Human-Environment Studies, Kyushu University : Master's program

Minami, Kosho
Department of Architecture, Graduate School of Human-Environment Studies, Kyushu University : Master's program

Kawano, Akihiko
Department of Architecture and Urban Design, Faculty of Human-Environment Studies, Kyushu University

他

https://doi.org/10.15017/1560202

出版情報：都市・建築学研究. 27, pp.73-83, 2015-01-15. Faculty of Human-Environment Studies, Kyushu University
バージョン：

都市・建築学研究　九州大学大学院人間環境学研究院紀要　第27号，　2015年１月
J. of Architecture and Urban Design, Kyushu University, No.27, pp. 73～83, January. 2015

Experimental Investigation on Dynamic Responses of Concrete-Filled Steel Tubular Members subjected to Transverse Impact Loads
衝撃横荷重を受けるコンクリート充填鋼管の動的応答に関する実験的研究

Mahmud Kori EFFENDI*, Hiromitsu KAWAGUCHI**, Kosho MINAMI**, Akihiko KAWANO***, Toshihiko NINAKAWA***, Shintaro MATSUO***, Keigo TSUDA**** and Masae KIDO****

マハムド コリ エフェンディ *，河口弘光 **，南　幸翔 **，河野昭彦 ***，
蜷川利彦 ***，松尾真太朗 ***，津田惠吾 ****，城戸將江 ****

Current Tsunami disaster events have indicated that the needs of Tsunami evacuation buildings. Such buildings should be designed to withstand not only wave pressure of Tsunami but also collision of flotsam carried by Tsunami. With respect to the wave pressure, the design method has been almost established where the loads by wave pressure are treated as statically equivalent loads. On the other hand, with respect to the collision of flotsam, the quantitative design method has not been established so far. In this paper, we carried out the impact loading test of concrete-filled steel tubular (CFT) members, so that CFT members may be expected to have effective resistance for Tsunami flotsam in comparison with steel members or reinforced concrete members, because CFT members can resist well against locally intensive loads at collision surfaces. For the comparison, vacant steel tubular members are also tested. Being based on the experimental results, we discuss the collapse modes, energy balance between input energy by impact loads and energy absorption capacity of CFT members, and the balance between the impulse and the momentum. In order to make clear dynamic effects in impact loading test, static loading test is conducted as well.

Keywords: Static Loading, Impact Loading, Input Energy, Energy Absorption, Impulse, Momentum
キーワード：静的載荷、衝撃載荷、入力エネルギー，吸収エネルギー，力積，運動量

1. Introduction

Current Tsunami disaster events have indicated that the needs of buildings that can be used as Tsunami evacuation buildings. In flat coastal areas, sometimes, there are no highlands for inhabitants to evacuate from Tsunami. Therefore, the Tsunami evacuation buildings or facilities are strongly recommended in such areas by the appropriate density.

One serious problem of Tsunami evacuation buildings and facilities is the collision of flotsam adding to the wave pressure by the Tsunami. With respect to the wave pressure, the design method has been almost established where the wave pressure loads are treated as statically equivalent loads. On the other hand, the quantitative design method has not been established for the collision phenomena of flotsam so far.

The impact transverse load is realized by dropping a striker in the experiment. The striker is composed of a hard steel loading head with spherical surface and a back up weight of a mild steel cylinder with mass of 125kg or 250kg. The striker is dropped to a specimen from a certain height. The collision velocity of the striker is here determined referring to the velocity of Tsunami flotsam. From the Tohoku Offshore Pacific Ocean Earthquake, the Tsunami flow velocity is reported as 7m/s in the river bank area in Natori, Miyagi Prefecture from the video analysis[1]. Therefore, the velocity of Tsunami flotsam must be the 7m/s, which is set on the experiment. Cantwell and Morton[2] classified that an impact velocity less than 10 m/s is the low velocity impact problem. Low velocity impact loading generates an overall mode of target response whereby energy can be dissipated at points well away from the point of contact, Fig. 1a. The high velocity impact loading induces a localized form of target response similar to that shown schematically in Fig. 1b where most of the energy is dissipated over a very small zone immediate to the point of impact.

In recent years, a number of researches has been conducted to study the impact behavior of the concrete-filled steel tubular (CFT) members through experimental analysis. R. Wang et al.[3], conduct a series of experimental studies to obtain the residual deformation

*　空間システム専攻博士後期課程
**　空間システム専攻修士課程
***　都市・建築学部門，九州大学
****　国際環境工学部，北九州市立大学

Table 1. Mechanical Properties of Specimens

Cross Section	Steel Tubes						Concrete	
	Type	Diameter or Width (*D* or *B*) mm	Thickness (*t*) mm	Yield Stress (N/mm^2)	Tensile Strength (N/mm^2)	Young's Modulus ($x10^5$) (N/mm^2)	Compression Strength (N/mm^2)	Young's Modulus ($x10^4$) (N/mm^2)
Circle	STK400	114.3	3.2	411	486	2.11	70.6	3.91
Square, Diamond	STKR400	100.0	3.0	385	485	1.89		

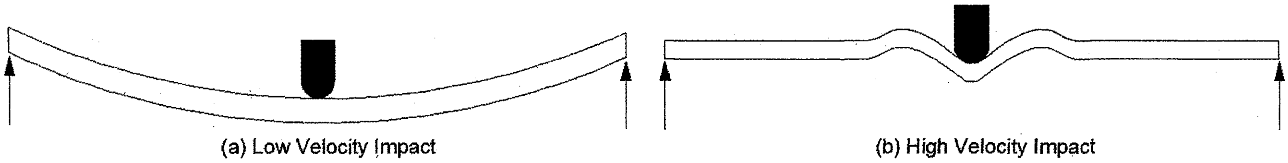

Fig. 1 Schematic Representation of the Impact Response under
(a) Low Velocity Impact Loading (b) High Velocity Impact Loading (After Cantwell and Morton[2]))

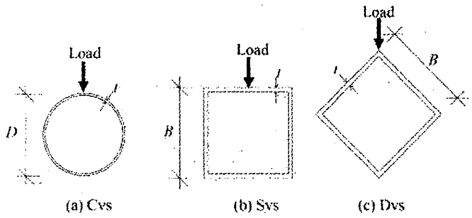

Fig. 2 Cross Sections of Tubular Members

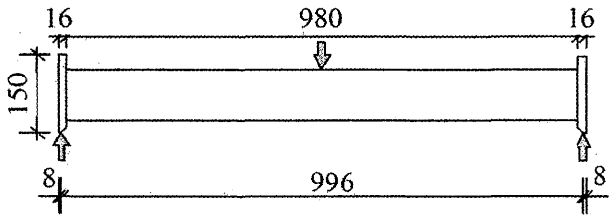

Fig. 3 Test Specimen (Unit: mm)

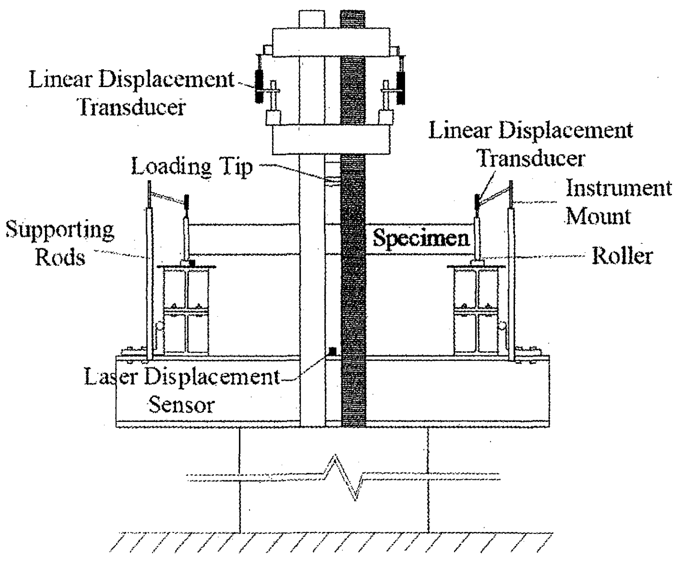

Fig. 4 Test Setup of Static Loading

mode and the time histories of impact loads. The testing parameters include, impact energy and the axial level (n) on CFT members. The results show that axial load level (n) on the CFT members has a significant effect on the impact force curves and the residual lateral deflection.

Deng et al.[(4)], carried out an experimental to study the CFT members, steel fiber-reinforced CFT members and post-tensioned CFT members under flexural load. The failure modes and local damages in those specimens have been investigated extensively. The experimental results are analyzed in the context of principles of energy and momentum conservation.

Uy and Remennikov[(5)] conduct an extensive experimental series to study the behavior of high performance steel sections subjected to transverse impact loads. The experimental program has considered both mild structural steel and stainless steel hollow sections both filled and unfilled being tested. The results also indicated a significant increase in not only capacity but also ductility and energy absorption capacity of hollow steel sections

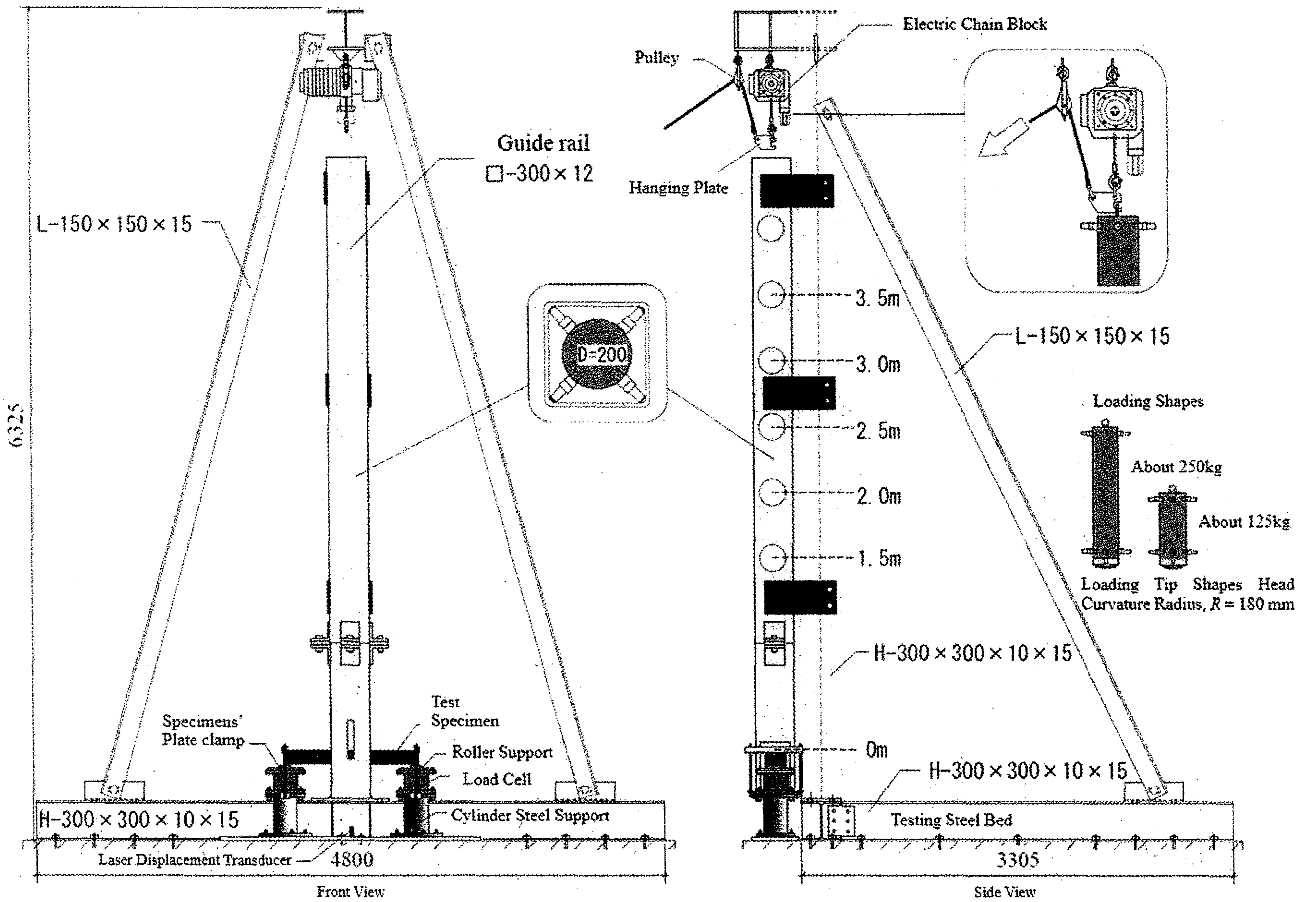

Fig. 5 Test Setup of Impact Loading

Table 2. Experimental Parameters

Specimen Names	Specimens	Test Method	*D* or *B* (mm)	*t* (mm)	Dropping Height (*H*) (mm)	Mass (*m*) (kg)
Cfi1	Circular CFT	Impact	114.3	3.2	2500	125
Cfi2					1250	250
Cfi3					2500	250
Cfs		Static			-	-
Cvi1	Circular Vacant Tubes	Impact			1250	125
Cvi2					1250	250
Cvs		Static			-	-
Sfi1	Square CFT	Impact	100.0	3.0	2500	125
Sfi2					1250	250
Sfi3					2500	250
Sfs		Static			-	-
Svi1	Square Vacant Tubes	Impact			1250	125
Svi2					1250	250
Svs		Static			-	-
Dfi1	Diamond CFT	Impact	100.0	3.0	2500	125
Dfi2					1250	250
Dfi3					2500	250
Dfs		Static			-	-
Dvi1	Diamond Vacant Tubes	Impact			1250	125
Dvi2					1250	250
Dvs		Static			-	-

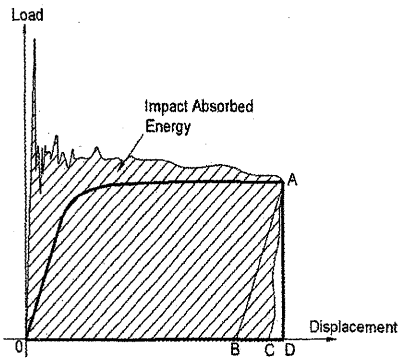

Fig. 6 Energy Calculation

utilizing concrete infill.

Therefore, we conduct the experimental work on CFT members subjected to transverse impact loads. Being based on the experiment, we will discuss the collapse modes, energy balance between input energy by impact loads and energy absorption capacity of CFT members, and the balance between the impulse and the momentum.

2. Specimens Overview

Specimens consist of three types of steel tubular members: square, circular, and diamond cross-sectional shapes. The steel tubular member of the diamond cross section means the case that Tsunami flotsam collides at the corner of the member of square cross section. CFT and vacant tubular members are used for each type of cross-sectional shapes. The steel materials are STKR400 and STK400 which are specified in the Japanese Industrial Standards (JIS) for square tubular members and circular tubular members, respectively. High-strength concrete f_c' = 70.6 N/mm^2 is used as infill material of CFT members.

The mechanical properties of the materials are indicated in Table 1. The cross sections of test specimens are shown in Fig. 2. Figure 3 shows the dimensions of test specimens, which may be thought about the one fifth to one tenth model of a real column in medium height multi-story buildings. Fifteen specimens are for impact loading test, and another six specimens are for static loading test. The test specimen's detail can be seen in Table 2.

3. Static Test[6)]

The test setup for static loading is illustrated in Fig. 4. The supports are basically pin and roller supports at both ends. Roller support is a simple one which is just greased between the bottom end plate of a specimen and testing bed which is made by H-shaped steel, so that specimen ends can freely slide in the member axis direction.

Two displacement transducers are installed to measure the displacement of a loading head, and a laser displacement sensor is placed at bottom of mid-span of a tubular member to measure the overall displacement. Strain gauges are installed at the bottom of mid and quarter span for a square tube and a circular tube. With respect to diamond tube, strain gauges are installed at center of plate elements at lower sides at mid and quarter span. The load is applied monotonically under displacement control of specimens.

4. Impact Loading Test [6)]

4.1 Dropping Height of a Striker

The impact loading test corresponding to the collision of Tsunami flotsam is performed by dropping a striker in the vertical direction to a specimen as shown in Fig.5. The input energy by a dropping striker is equal to its gravitational potential energy. From the start of collision of the striker and a specimen, the potential energy is converted into the kinematic energy according to the energy principle as follows.

$$mgH = \frac{1}{2}mv^2 \quad (1)$$

Where, v is the velocity of the striker at the beginning of the collision, g is the gravitational acceleration, and H is the dropping height of the striker. From Eq. (1), the following equation is derived.

$$H = \frac{v^2}{2g} \quad (2)$$

From one of the findings from the Tohoku Offshore Pacific Ocean Earthquake, the velocity of Tsunami flotsam may be as 7m/s in a usual case. The corresponding H of 2.5m is derived from the velocity of 7m/s by Eq. (2).

4.2 Mass of the Striker in the Experiment

In order to determine the mass magnitude of striker in the experiment, the target is introduced for residual deformation of CFT specimens. The target is set at 5% of the span length L, where the member is expected to deform up to the full plastic range.

Being based on the above condition, the plastic energy, or the energy absorption capacity of a specimen corresponding to the residual deformation target, $E_{OP(5\%)}$ is calculated by the following equation.

$$E_{OP(5\%)} = P_u(0.05L) \quad (3)$$

Where, L (=996mm) is the span of a specimen, and P_u is the transverse load at full plastic state of a specimen. From the plastic collapse mechanism of a specimen under the condition as shown in Fig. 3, the plastic collapse load of the transverse load P_u is expressed as follows:

$$P_u = \frac{4Mu}{L} \quad (4)$$

Where, M_u is the full plastic moment. The requirement of mass magnitude of a striker m_{req} should satisfy the following energy balance.

$$m_{req}gH = E_{OP(5\%)} \quad (5)$$

From the Eqs. (3), (4) and (5), the m_{req} is determined as follows:

$$m_{req} = \frac{0.2M_u}{gH} \quad (6)$$

Being based on the full plastic moment of a circular CFT

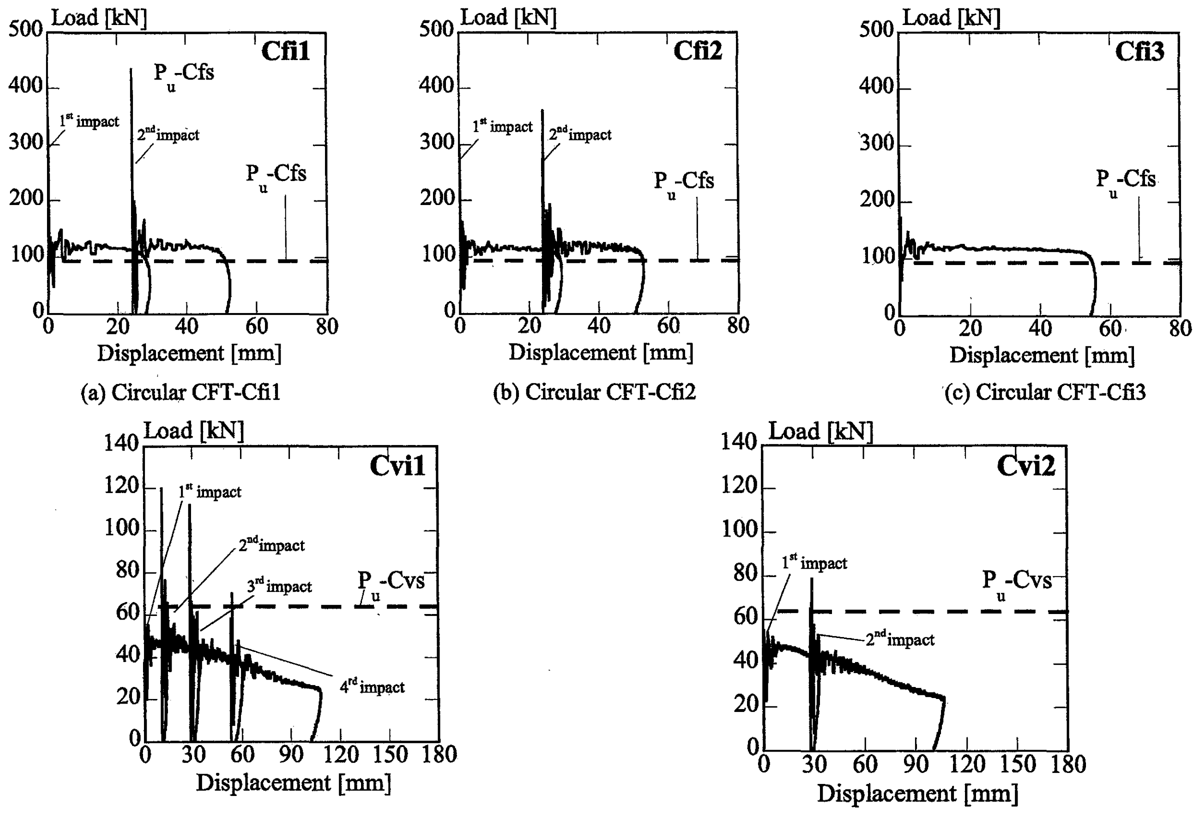

(a) Circular CFT-Cfi1 (b) Circular CFT-Cfi2 (c) Circular CFT-Cfi3

(d) Cvi1 Specimens (e) Cvi2 Specimens

Fig. 7 Load-displacement Relationships of Circular CFT and Circular Vacant Specimens by Experiment and Theoretical Full Plastic Strength

member, the m_{req} is determined as 125kg (for H=2.5m, v=7m/s), and 250kg (H=1.25m, v=5 m/s), respectively.

4.3 Apparatus for Impact Loading Test

The impact loading test is performed using the experimental apparatus as shown in Fig. 5. The striker of mass of 125kg or 250kg drops inside of a square steel tube which works as a vertical guide rail. The contact head of the striker has a shape of hemispherical with the curvature radius of 180mm.

The reaction forces at both ends of a specimen are measured by load cells of 1000kN capacity, which are installed at the both ends of the specimen. The deflection of the mid span of the specimen is measured by a laser displacement transducer with the sampling period of 0.00033 second.

5. Energy Equilibrium

5.1 Absorbed Energy by specimen

Typical transverse load-deflection relationships of a CFT specimen observed in the impact loading test and the static loading test are shown in Fig. 6. The absorbed energy of the specimen is obtained from the integrated area of the transverse load-deflection relationship. The area of OABO in Fig. 6 represents plastically absorbed energy in the static loading test. The curve with some turbulence represents the result by impact loading test. The absorbed energy of a specimen in the impact loading test is somewhat larger than that in the static loading test. This is caused by the inertia forces, damping forces and the material strength increase by high strain rates. The comparison between dynamic and static energy absorptions is done under the condition that the residual deflections of both tests are same, in which the stiffness of unloading process in the static loading test is assumed to be the initial elastic stiffness.

5.2 Input Energy by a Striker

The input energy of a striker is its gravitational potential energy, which is determined by the mass and the dropping height. Rigorously speaking, the height of the striker should take the account of the displacement after collision up to the zero velocity δ_{max}. The input energy by the striker E_i is as follows:

$$E_i = mg(H + \delta_{max}) \tag{7}$$

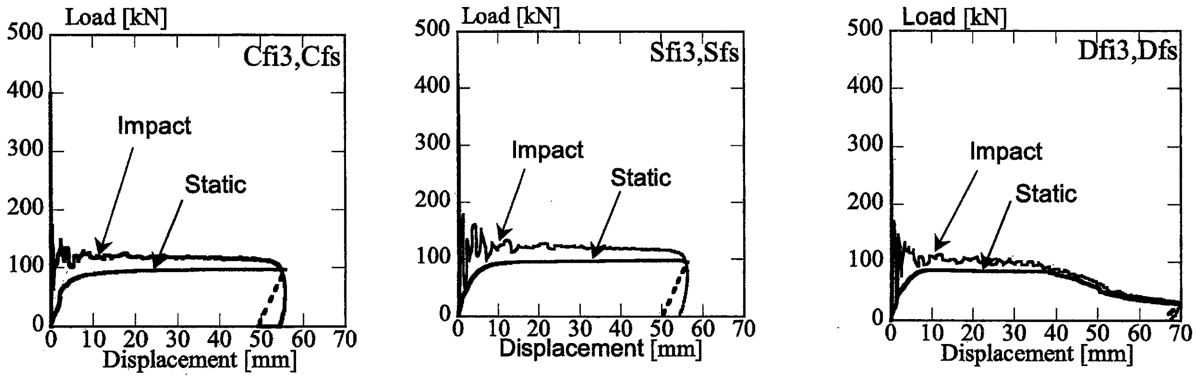

(a) Circular CFT (b) Square CFT (c) Diamond CFT

Fig. 8 Comparison of Transverse Load-Deflection Relationship of CFT specimens of Impact Loading and Static Loading

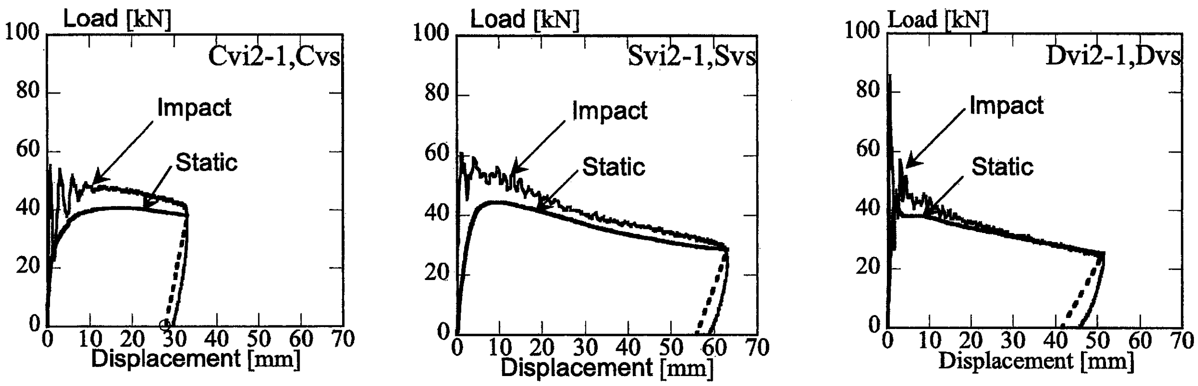

(a) Circular Vacant Member (b) Square Vacant Member (c) Diamond Vacant Member

Fig. 9 Comparison of Transverse Load-Deflection Relationship of Vacant Steel Tubular Specimens of Impact Loading and Static Loading

The E_i should satisfy the following equilibrium equation.

$$E_i = E_{OP} + E_E + E_{LP} + E_V \qquad (8)$$

Where, E_{OP} is the absorbed energy of a specimen by the global plastic deflection and the local plastic deformation caused by the striker's head. E_E is the elastic strain energy or vibration energy of a specimen, E_{LP} is the absorbed energy by local buckling or instable deformation of steel tubular walls. E_V is the absorbed energy by stress wave propagation which may be small because the impact loading test is classified as the low velocity collision. E_E and E_{OP} can be directly calculated by integrating the area of the load-deflection relationships in the experiment.

6. Experimental Results and Discussions

6.1 Transverse Load-Deflection Relationships in Impact Loading Test

Figure 7 shows the relationships between the transverse load and deflection under impact loading test, which are derived by combining the deflection-time relationships and the transverse load-time relationships. The transverse load is measured by reaction forces at both end supports of a specimen. We have investigated the direct impact forces of striker by using accelerometer which is attached to the striker. The result supports the accuracy of the reaction forces at the end supports.

At the beginning of the collision, the extremely high pulse load is observed for each specimen. Although after the beginning of the collision, the load vibrates, but it converges to a constant load. The constant transverse load is the full plastic strength of the specimen.

Figures 7(a) and 7(b) represent the relationships of circular CFT members Cfi1 and Cfi2, respectively. Both specimens are subjected to striker's collision twice. For the Cfi1, the mass m and dropping height H of the striker are 125kg and 2500mm, respectively. For the Cfi2, the m and H of the striker are 250kg and 1250mm, respectively. What we should pay attention to is that input energy, that is, the gravitational potential of the strikers are same in Cfi1 and Cfi2, even though the masses and heights of strikers are

Table 3. Absorbed Energy of Specimens and Input Energy by Strikers

Specimen Names	Specimens	Test Method	*D* or *B* (mm)	*t* (mm)	Dropping Height (*H*) (mm)	Mass (*M*) (kg)	Maximum Deflection (mm)	Residual Deflection (mm)	$E_{OP}+E_E$ (J) (a)	E_I (J) (b)	Energy Ratio (a)/(b) (%)
Cfi1-1	Circular CFT	Impact	114.3	3.24	2500	125	29.3	23.9	3324	3526	94.3
Cfi1-2							52.2	46.6	3242	3558	91.1
Cfi2-1					1250	250	29.2	23.3	3260	3351	97.3
Cfi2-2							52.8	46.6	3323	3413	97.4
Cfi3					2500	250	55.7	49.2	6434	6696	96.1
Cfs		Static			-	-	55.7	-	4995	-	-
Cvi1-1	Circular Vacant Tubes	Impact			1250	125	14.1	10.6	599	1762	34.0
Cvi1-2							33.7	28.5	1010	1789	56.5
Cvi1-3							60.5	52.7	1267	1827	69.4
Cvi1-4							108.1	96.5	1646	1893	86.9
Cvi2-1					1250	250	33.0	27.9	1425	3361	42.4
Cvi2-2							106.8	95.1	2636	3554	74.2
Cvs		Static			-	-	33.0		1248	-	-
Sfi1-1	Square CFT	Impact	100	3.01	2500	125	29.9	24.2	3433	3527	97.3
Sfi1-2							54.4	48.4	3506	3561	98.5
Sfi2-1					1250	250	29.7	24.1	3369	3353	100.5
Sfi2-2							53.5	47.4	3398	3415	99.5
Sfi3					2500	250	56.3	50.1	6688	6697	99.9
Sfs		Static			-	-	56.3		5101	-	-
Svi1-1	Square Vacant Tubes	Impact			1250	125	21.9	17.4	1099	1773	62.0
Svi1-2							61.5	54.6	1575	1828	86.1
Svi1-3							136.2	126.5	2066	1932	106.9
Svi2-1					1250	250	63.1	55.9	2568	3440	74.7
Svi2-2							230.0	230.0	4150	3877	107.0
Svs		Static			-	-	63.1		2237	-	-
Dfi1-1	Diamond CFT	Impact	100	3.01	2500	125	29.9	24.5	3144	3527	89.2
Dfi1-2							56.8	51.0	3260	3564	91.5
Dfi2-1					1250	250	29.3	23.7	2951	3352	88.0
Dfi2-2							57.8	52.2	3082	3426	90.0
Dfi3					2500	250	69.8	65.6	5690	6732	84.5
Dfs		Static			-	-	69.8		4602	-	-
Dvi1-1	Diamond Vacant Tubes	Impact			1250	125	17.7	12.7	729	1767	41.3
Dvi1-2							47.8	38.2	1085	1809	60.0
Dvi1-3							95.2	80.1	1217	1875	64.9
Dvi2-1					1250	250	51.5	41.6	1729	3410	50.7
Dvi2-2							232.0	232.0	3344	3882	86.1
Dvs		Static			-	-	51.5		1648	-	-

different. Figures 7(a) and 7(b) demonstrate the residual deflection for each collision is almost same regardless of the first and the second collisions nor differences of the striker's properties. Therefore, of course, total residual deflection is obtained by adding that in each collision.

Figure 7(c) indicates the specimen Cfi3 to which the striker with m=250kg and H=2500mm collides only once. The striker for Cfi3 has the gravitational potential energy twice as large as Cfi1 or Cfi2. It is noteworthy that the residual deflection of Cfi3 is almost same as the total those of Cfi1 and Cfi2. The same phenomena are found in the square CFT specimens Sfi1, Sfi2 and Sfi3, and the diamond cross sectional shaped CFT specimens Dfi1, Dfi2 and Dfi3, although they are not shown here on account of the space.

Figures 7(d) and 7(e) denote the vacant circular steel tubular specimens Cvi1 and Cvi2, respectively. The striker for the Cvi1 is comprised of the mass of 125kg and the dropping height of 1250mm. The Cvi1 has the collisions by striker four times. The transverse load deteriorates as the number of times of the collision increases. Simultaneously, the incremental quantity of residual deflection increases.

The striker for the Cvi2 has the mass of 250kg which is

Table 4. Collapse Mode of Specimens under static loading

		
(a) Cvs	(b) Svs	(c) Dvs
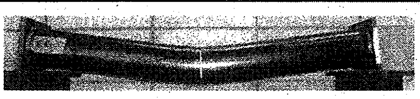	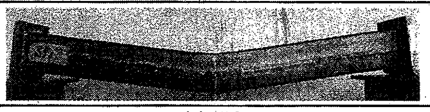	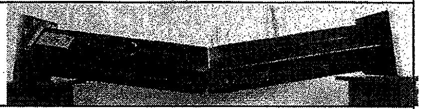
(d) Cfs	(e) Sfs	(f) Dfs

twice as large as that of Cvi1, and the dropping height of 1250mm is same as that of Cvi1. Therefore, the input energy for Cvi2 is twice as large as that for Cvi1. Under these conditions of the strikers, total residual deflection of Cvi1 after four times collisions is almost same as that of Cvi2 after twice collisions. The same phenomena are found for the square vacant steel tubular specimens Svi1 and Svi2, and the diamond cross sectional shaped vacant steel tubular specimens Dvi1 and Dvi2.

6.2 Comparison of Transverse Load-Deflection Relationships between in Impact Loading Test and in Static Loading Test

The transverse load-deflection relationships of CFT specimens under impact loading are compared with those under static loading in Fig. 8, where the static relationship is cut off so as to be the same residual deflection of corresponding specimen under impact loading. The unloading stiffness is assumed as the initial elastic stiffness.

As shown in Fig. 8, the transverse load of a specimen under impact loading is higher than that of corresponding one under static loading. The difference between the loads of specimens under impact loading and under static loading is caused by the inertia forces, viscous damping resistance, and the material property such that the yield strength and the maximum strength increase as the strain rate increases. The estimated strain rate is over 100%/sec.

In Fig. 9, the comparison is indicated for the behaviors of vacant steel tubular specimens under impact loading and under static loading. Similar to the case of CFT specimens, the transverse load of a vacant steel tubular specimen under impact loading is higher than that of the corresponding one under static loading. The load increase can be explained by the same reasons as the case of CFT specimens. The negative slope is observed after the peak load, where the slope of a specimen under impact loading is almost same as that of one under static loading. The strength reduction is caused by the local deformation of tubular walls in the contact area by the striker and the local buckling of tubular walls by in-plane compression.

6.3 Comparison between Input Energy by Striker and Absorbed Energy of Specimen

In Table 3, the absorbed energy by a specimen $E_{OP}+E_E$ is compared with the input energy by a striker E_i. Generally speaking the ratio of $E_{OP}+E_E$ to E_i of each specimen has a tendency to be less than 1.0. One of the reasons is the energy loss by stress wave propagation E_V which is not taken into account. Another reason is that the $E_{OP}+E_E$ is derived from the integration of the transverse load in the mid-span deflection which does not include the absorbed energy by local deformation of tubular walls or local crush of infill concrete.

With respect to circular CFT specimens (Cfi1, Cfi2, Cfi3) and square CFT specimens (Sfi1, Sfi2, Sfi3), the ratio of $(E_{OP}+E_E)/E_i$ is slightly smaller than 100% in each, so that the input energy is almost balanced with absorbed energy. With respect to diamond cross sectional shaped CFT specimens (Dfi1, Dfi2), the ratio of $(E_{OP}+E_E)/E_i$ is around 90% which is smaller than those of circular and square CFT specimens. This may be thought that the striker collides against a corner of a square tube with a local crush which absorbs a part of the impact energy. The ratio of Dfi3 is the least in CFT specimens, so that the crack appears at the steel tubular bottom side, which is a corner of a square tube, during the impact loading procedure.

With respect to vacant steel tubular specimens (Cvi1, Cvi2, Svi1, Svi2, Dvi1 and Dvi2, the ratio of $(E_{OP}+E_E)/E_i$ is much lower than those of CFT specimens. The lowest ones are vacant circular tubular specimen (Cvi1, Cvi2). This is because that the cross section of a circular tube subjected to the concentrated contact pressure is easy to flatten and to lose the member flexural stiffness. It is noteworthy that the ratio of $(E_{OP}+E_E)/E_i$ increases as the number of collisions by the striker increases. This is because that vacant steel tube deforms locally at first, and then the overall flexure progresses.

Table 5. Collapse Mode of Specimens under Impact Loading

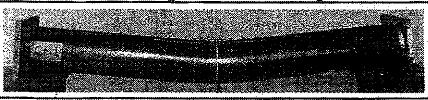	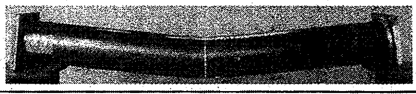	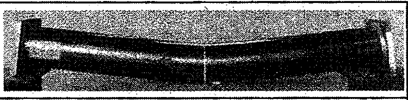
(a) Cfi1-2	(b) Cfi2-2	(c) Cfi3
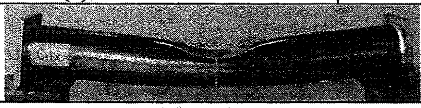	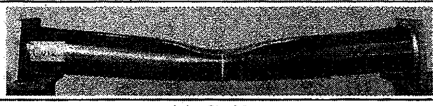	
(d) Cvi1-2	(e) Cvi2-1	
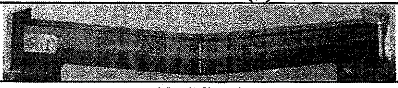	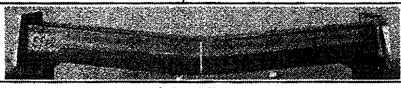	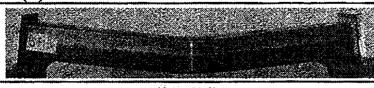
(f) Sfi1-2	(g) Sfi2-2	(h) Sfi3
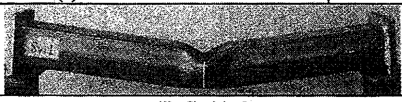	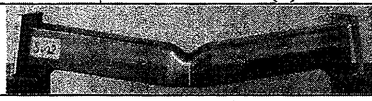	
(i) Svi1-2	(j) Svi2-1	
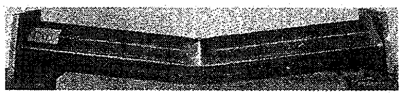	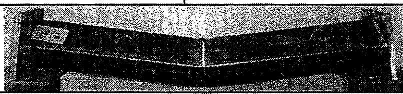 	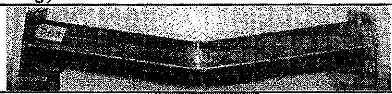 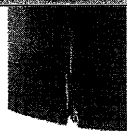
(k) Dfi1-2	(l) Dfi2-2	(m) Dfi3
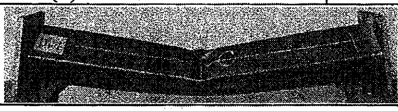	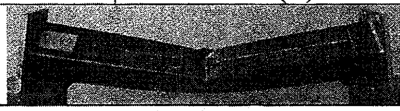	
(n) Dvi1-2	(o) Dvi2-1	

6.4 Collapse Modes

Table 4 indicates the collapse modes of specimens after static loading test. Photographs from (a) to (c) in Table 4 are vacant steel tubular specimens. The collapse modes are the flexural deflection with local deformation and/or local buckling. The figure of the local deformation of circular steel tubular specimen Cvs is a copy of striker's head, where the figure of loading head in a static loading test is same as striker's head in an impact loading test. With respect to square vacant tubular specimen Svs and diamond shaped vacant steel tubular specimen Dvs, it is observed the local buckling mode which is different figure from the striker's head as well as flexural deflection and local deformation of striker's head copy.

The collapse mode of CFT members under static loading is flexural deformation in the mid span with almost no local deformation or no local buckling as shown in (d) to (f) in Table 4.

Table 5 indicates the collapse modes of specimens after impact loading test. The collapse modes of CFT specimens and vacant steel tubular specimens under impact loading are almost similar to those of corresponding specimens under static loading.

Cracks appear at the bottoms of steel tubes of diamond tubular specimens Dfi2 in the photographs (l) and Dfi3 in (m), which received totally the same and large amount of input energy from the striker. The similar collapse mode can be seen in the specimen Dfs under static loading in photograph (f), which residual deflection exceeds those of the Dfi2 or the Dfi3. On the other hand, there is no crack found in the Dfi1 as shown in the photograph (k), which has received only half of the input energy of Dfi2 and Dfi3. Therefore, it can be said that the cracks of tubular walls are determined by the amount of input energy or residual deflection.

6.5 Impulse and Momentum

The time integration of the impact force is the impulse, which is equal to the momentum as shown in Eq. (9).

$$\int_0^{\Delta t} P dt = mv \qquad (9)$$

Where, P is the impact force, t is time, m is mass of the striker, v is the change of velocity of the striker and Δt is the duration time of collision. As shown in Fig. 6, the transverse load is equal to the full plastic strength and is kept to be P_u.

Therefore, the impulse can be approximately expressed

Table 6. Momentum of the Striker and Impulse of Specimens

Specimen	Dropping Height (H) (mm)	Mass of Striker (m) (kg)	Collision Duration Period Δt (ms)	Impulse $F\Delta t$ (kN . sec) (a)	Momentum $m\sqrt{2gH}$ (kN. sec) (b)	Impulse Momentum Ratio (a) /(b)
Cfi3	2500	250	20.15	2.27	1.87	1.21
Cvi2-1	1250	250	33.9	1.44	1.32	1.09
Sfi3	2500	250	19.50	2.24	1.87	1.19
Svi2-1	1250	250	38.35	1.56	1.32	1.18
Dfi3	2500	250	28.80	1.95	1.87	1.04
Dvi2-1	1250	250	42.4	1.36	1.32	1.03

as:

$$\int_0^{\Delta t} Pdt = P_u \Delta t \tag{10}$$

Simultaneously, by using Eq. (2), the momentum of the striker can be expressed as the following equation.

$$mv = m\sqrt{2gH} \tag{11}$$

From Eqs. (9), (10) and (11), the following approximation relationship is obtained.

$$P_u \Delta t = m\sqrt{2gH} \tag{12}$$

In the impact loading test, the specimen strength increases from the P_u because of the material properties affected by strain rates, damping forces and inertia forces. Therefore, the averaged dynamic transverse resistance F is introduced in substitution for the P_u, as follows:

$$F\Delta t = m\sqrt{2gH} \tag{13}$$

In Table 6, the $F\Delta t$ is the impulse where F is the averaged dynamic transverse resistance and Δt is the collision duration period. Both of F and Δt are observed in experiment. On the other hand, $m\sqrt{2gH}$ is the momentum calculated by striker's mass m and its dropping height H, that is the theoretical value from the striker's potential. The ratio of $F\Delta t$ to $m\sqrt{2gH}$ shown in Table 6 is almost 1.0. In other words, the momentum of the striker is successfully converted into the impulse of the specimen regardless of CFT and steel tubular members.

From the agreements between the theoretical momentum and the experimental impulse, the duration periods of the collision Δt derived from the experiment by using Eq. (13) must be correct. With respect to the scale of this experiment, Δt are from 20 seconds to 40 seconds.

7. Conclusive Remarks

The impact transverse loading test is carried out for the total number of 15 CFT and vacant tubular specimens. In order to investigate the dynamic effects, the static transverse loading test is also performed for the total number of 6 specimens. From these test, conclusive remarks are as follows:

(1) In the impact loading test, at the beginning of collision, the extremely high pulse load is observed for every specimen. After that, the load vibrates for a while, and finally it converges to a constant load which is the full plastic strength of the specimen.

(2) The residual deflection of a specimen is determined by the total input energy of the striker to the specimen. For example, the residual deflection of the specimen subjected to the two collisions by a striker is almost same as that subjected to the one collision by another striker which has the twice energy. This phenomenon is true for both of CFT specimens and vacant steel tubular specimens. However, with respect to vacant steel tubular specimens, the transverse load deteriorates as the number of times of the collision increases, and the incremental quantity of residual deflection increases.

(3) The transverse load of a specimen under impact loading is higher than that of the corresponding specimen under static loading. The difference is caused by the inertia forces, viscous damping resistance, and the material property changes such that the yield strength and the maximum strength increase as the strain rate increases.

(4) The validity of the impact loading procedure by the dropping strikers of masses of 125kg and 250kg are confirmed by the energy balance between the input energy by a dropping striker's gravitational potential energy, and the absorbed energy of a CFT specimen which is integrated area of a transverse load-deflection

relationship in the experiment. The absorbed energy of a CFT specimen shows a little bit smaller than the input energy by a striker, by the energy loss of the stress wave propagation and so on. With respect to vacant steel tubular specimens, the absorbed energy is much smaller than the input energy, because of local deformation and/or local buckling. It is noteworthy that the ratio of the ratio of the absorbed energy to the input energy increases as the number of collisions by the striker increases. This is because that vacant steel tube deforms locally first, and then the overall flexure progresses.

(5) The collapse modes of CFT and vacant steel tubular specimens under impact loading are basically the same as those of under static loading test. The collapse modes of CFT members are flexural deformation in mid span of specimens with slight local deformation of steel walls in compression side. With respect to the diamond shaped CFT specimens, cracks appear in steel walls at the bottom corners. The collapse mode of a circular vacant tube is flexural deformation with local deformation of copy of striker's head. The mode of square and diamond shaped vacant tubular specimens is the flexural deformation with local deformation and local buckling.

(6) The validation of the impact loading test is also proved by a good agreement between the impulse obtained by experiment and the momentum calculated by the striker's potential energy.

Acknowledgement

This study is financially supported by the Scientific Research Grant (B) H25- H27 No. 25289186, Steel structure research and educational grant project H25, Ministry of Education, Culture, Sports, Science and Technology, Japan. One of the authors thanks the Indonesian Directorate of Higher Education Program (DIKTI) for a doctoral scholarship.

References

1) National Institute for Land and Infrastructure Management, Ministry of Land, Infrastructure, Transport and Tourism Building Research Institute, Incorporated Administrative Agency, Building Research Data No. 132 May 2011: Quick Report of the Field Survey and Research on "The 2011 off the Pacific coast of Tohoku Earthquake" (The Great East Japan Earthquake). (in Japanese)

2) G Cantwell WJ, Worton J. (1989), Comparison of the low and high velocity impact response of CFRP. Composites 1989;20(6):545–51.

3) Wang R, Han L-H, Hou C-C. (2012), Experimental study on the behaviour of concrete filled steel tubular (CFST) members under lateral impact, WIT Transactions on the Built Environment; 126:241–8

4) Deng Y, Tuan CY, Xiao Y. (2012), Flexural behavior of concrete-filled circular steel tubes under high-strain rate impact loading, J Struct Eng;138 (3):449–56.

5) Uy, B., & Remennikov, A. (2007), Behavior of high performance steel sections subjected to impact loads. Paper presented at the 5th International Conference on Advances in Steel Structures, December 5-7, Singapore.

6) Zaitsu Shūhei, et al (2014), An Experimental Study on the Behavior of Concrete Filled Steel Tubular Members under Tsunami Flotsam Impact Load(Part2)Experimental Result and Consideration , AIJ Kyushu Chapter Architectural Research Meeting, No. 53, pp. 557-560, March, 2014. [in Japanese]

（受理：平成26年11月13日）